Presented at the 9th Annual Conference on Iron and Steel Technology, Pohang, Korea, August 1997

Dynamic Behavior of Gas Metal Arc Welding

L. A. Jones, P. Mendez, D. Weiss, and T. W. Eagar
Massachusetts Institute of Technology
DMSE, Cambridge, MA 02139, USA

Abstract

Gas Metal arc Welding (GMAW) has become the most widely used process for joining of steel plates due to its high productivity, simplicity of equipment and ease of use. Although the process of melting of the electrode and development of the weld deposit has been studied for 40 years, the dynamic nature of the process has not been studied in detail because accurate models are computationally intensive and experiments to measure what is occurring in the arc are difficult due to the intense heat and light. In this presentation, the fundamentals of the GMAW process will be reviewed, followed by a detailed description of droplet formation and detachment followed by current studies of fluid behavior in the weld pool. It will be shown that fluid motion both within the drop and the weld pool has a significant effect on the quality of the weld produced.

1 Introduction

1.1 Simulation of transport phenomena in GMAW

The welding environment is characterized by extreme conditions such as high temperatures, intense light emitted from the plasma and the existence of multi-phase systems which make it particularly difficult or even impossible to measure values of interest with a high precision. With the rapid development of computing power and advanced numerical solution techniques new possibilities are opened up to predict transport phenomena associated with GMAW. Numerical simulation can be a suitable tool to gain insight in the determining processes and to reduce the experimental expense of the development of welding methods. However, computer analysis cannot explain more than the physics of the formulated mathematical model. A critical review of the hypothesis is needed on the basis of validation experiments.

1.2 Investigated welding method

GMAW is characterized by an electric arc as the heat source for melting of the base metal and the consumable electrode. The electrode is continuously fed to the arc and fills the groove of the base plate. The molten metal is protected from the atmosphere by the shielding gas (usually pure argon (Ar) or pure carbon dioxide (CO_2), or mixtures of Ar, CO_2, or oxygen (O_2)). The electric current is carried by a plasma consisting of ionized shielding gas.

The metal transfer mode affects the arc stability, fume generation, spatter, penetration, and the weld pool behavior and is of practical interest due to its essential influence on the weld quality. In principle free-flight metal transfer can be divided into two transfer modes [20]

- globular mode (drop, repelled) and
- spray mode (drop, projected, rotating, streaming, pulse).

The most important parameters influencing the transfer mode are the welding current I, arc voltage U, contact to workpiece distance CTWP, shielding gas composition, gas flow rate $\dot{V}_{gas}$, electrode/torch angle, alloying elements,

Table 1: Materials and welding parameters

	material	
electrode	ER70S-3 (bare)	
shielding gas	98% Ar + 2% O_2	
base metal	mild steel	
parameter	**range**	
I	180 – 480	A
U	27 – 35	V
$CTWP$	18 – 25	10^{-3} m
$\dot{V}_{gas}$	1.42	m^3 / h
D_{wire}	1.6	10^{-3} m

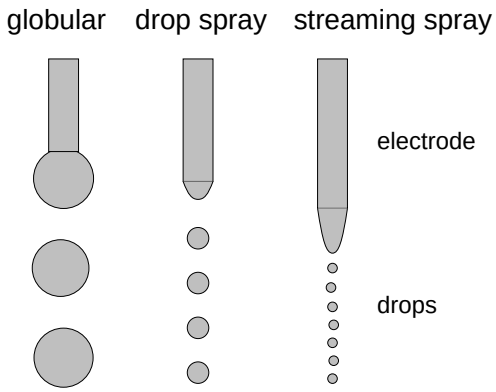

Figure 1: Drop transfer modes

wire feed speed v_{wire}, extension l_{wire} and diameter D_{wire} of the wire. The materials and the parameter range considered in the current work are given in Table 1. The welding current can be constant or pulsed.

The globular, drop (or projected) spray and steaming spray transfer mode can be observed in Figure 1. The character of the metal transfer depends mainly on the welding current, wherein the size of the drops decreases with an increasing current. In globular transfer the diameter of the spherical drops is greater than the electrode diameter. With increasing current the mode changes into drop spray transfer which is characterized by an acceleration of the drops. The drop shape is similar to globular transfer but with a diameter slightly smaller than the electrode. Upon a further increase in wire feed speed, the mode turns into streaming spray transfer characterized by very small drops, wherein an almost continuous column extends from electrode to base metal [9].

1.3 Analysis of the general problem

Modeling metal transfer in GMAW is a challenging task, since it involves a strong interdependence of the processes in the electrode, the plasma, and the weld pool region. One has to consider coupled transport phenomena influenced by combined electrical, magnetic, and chemical effects, free surface problems, and phase transitions. Figure 2 shows a schematic description, where the thin arrows stand for a small influence, while the thick arrows stand for a strong influence between the subproblems. Due to the relatively small influence of the processes in the weld pool on drop detachment and transfer it seems possible to decouple these subproblems. Thus three relatively independent regions of

1. drop formation and detachment,
2. processes in the arc column including the free flight of drops, and
3. drop impingement and weld pool behavior

can be considered.

One is faced with modeling problems such as an unsatisfactory knowledge of the material properties in the range of high temperatures, the existence of free surfaces, a multi-phase system, and extreme non-linearities in the describing equations and boundary conditions. That is why also the most sophisticated modeling efforts are restricted to small intervals of the welding parameters or they have to simplify the governing equations.

Many previous models focused on globular drop detachment from the electrode and small weld pool deformations. But globular drop transfer is rarely used in production. Due to

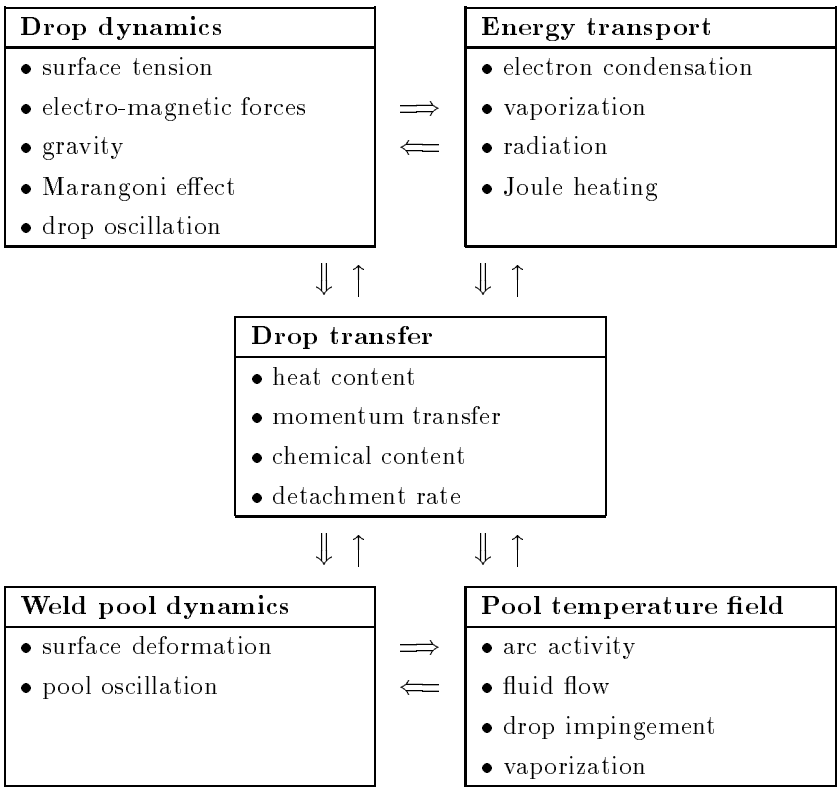

Figure 2: Partial problems

the small influence of the electromagnetic force, the drops are not accelerated towards the pool which leads to shallow and broad weld beads. High productivity applications involve the use of high currents with great weld pool deformations and impinging drops with significant momentum. That is why special emphasis should be given to the spray transfer mode of GMAW.

2 Previous modeling efforts

A classification of GMAW modeling efforts was proposed in [13]. The sub-models for electrode, arc, and weld pool region are named as first generation models (cf. Figure 3). They are focused on the modular development of models for the electrode [12, 31], arc [14, 18, 33], and weld pool region [15, 29, 32]. Approaches for the development of the resulting microstructure [2, 19], hydrogen diffusion [7, 25], and residual stress and distortion [8,28] are coupled with the weld pool behavior. Second generation models consider the interaction between electrode–arc [4,27], arc–pool [3,6], or electrode–arc–pool [23,35]. Proposed third generation models with inclusion of micro-modeling of solidification and solid weld mechanics in second generation models have not yet been acchieved.

Presently, there is a thorough understanding of the mechanism of drop detachment during globular transfer and of the behavior of the arc and of the weld pool for relatively small surface deformations. There has also been extensive modeling on the depression and the transport phenomena in simpler gas tungsten arc (GTA) or laser weld pools [5, 21, 30, 34].

There is a lack of understanding of the dynamics of the drop detachment and weld pool behavior during the high current regime of GMAW. For example, phenomena such as finger penetration (Figure 4) are still not understood. Weld defects such as undercutting, humping, and tunnel porosity are created by the interplay of processes occurring in the weld

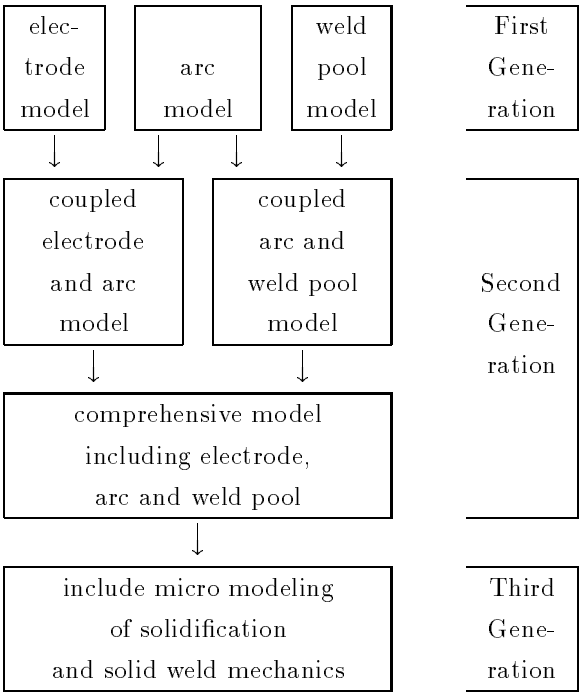

Figure 3: Classification of GMAW models (after [13])

pool, but there is no clear understanding of the fluid flow within the weld pool which leads to these defects (cf. Figure 5–7 with examples for these effects in GTAW).

The motivation of this paper is to make a contribution to better understanding of dynamics ruling these phenomena. Two models of the drop and weld pool region will be developed which are semi-coupled with a reduced model for the arc region describing the density of welding current and heat flux.

3 Drop Formation and Detachment

3.1 Modeling

The process of drop formation and detachment is characterized by a combined spatial and temporal nature and can be divided in the stages

1. melting of the electrode,
2. tapering of the electrode,

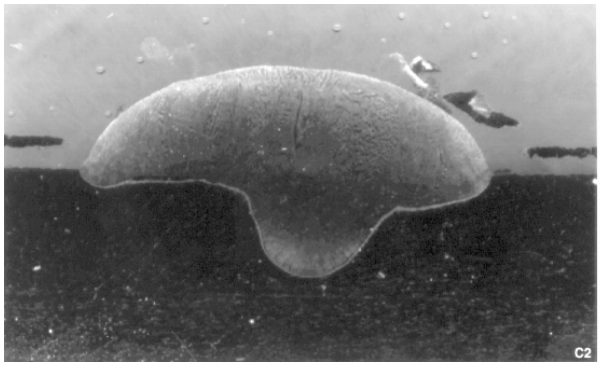

Figure 4: Finger penetration (from [24])

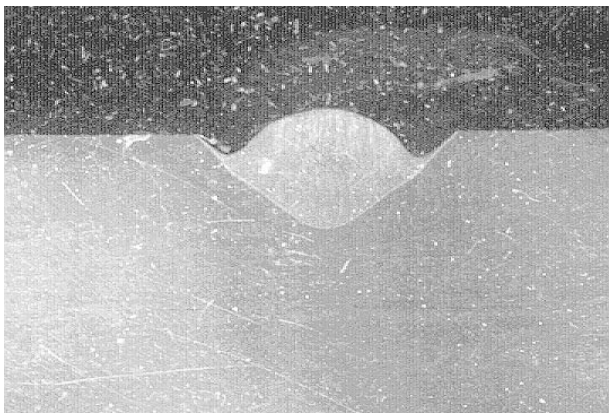

Figure 5: Undercutting (from [24])

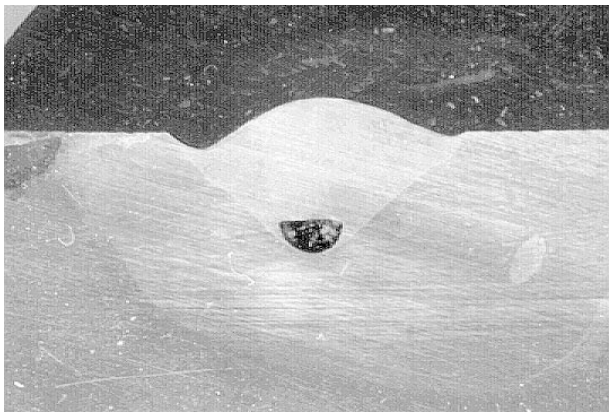

Figure 6: Tunnel porosity (from [24])

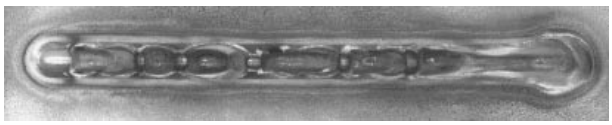

Figure 7: Humping (from [24])

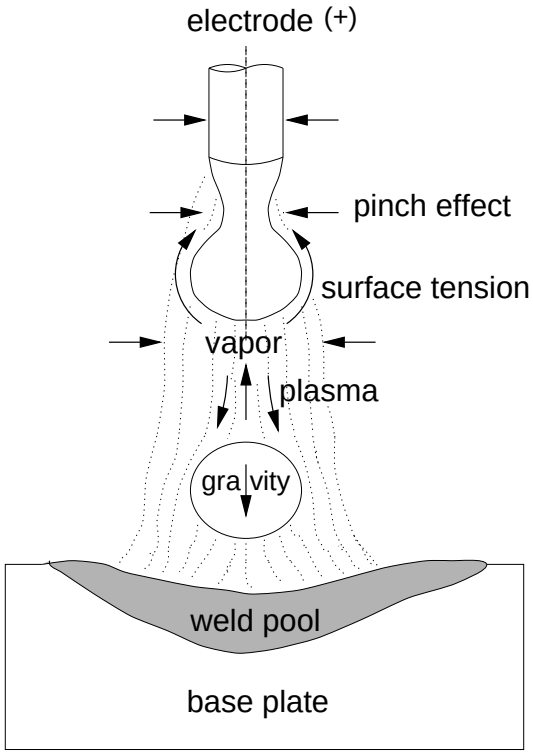

Figure 8: Forces acting on the drop

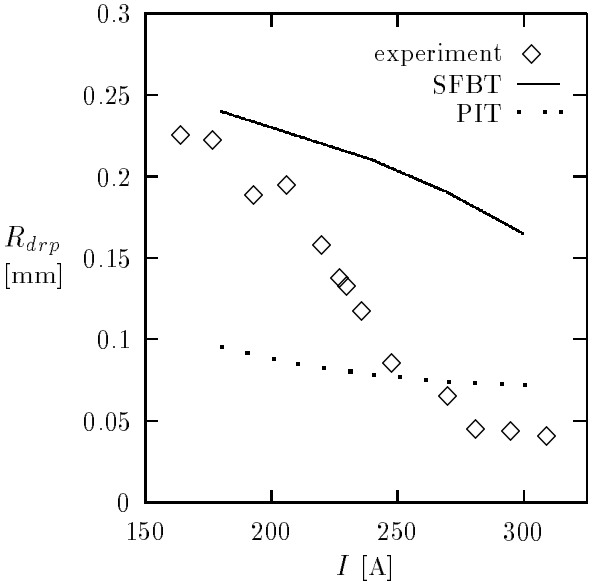

Figure 9: Comparison of experimental results and theoretical prediction using SFBT and PIT (from [17])

3. formation of the drop, and
4. pinching off the drop.

The thermal processes in stage (1) and (2) determine the position of the melting interface between wire and drop and the volume of the pendant drop. Because these data are available from experiments [16], this investigation will be focused on stage (3) and (4). The detaching forces involved are (cf. Figure 8)

- electromagnetic force F_{mag},
- gravitational force F_g,
- aerodynamic drag force (shear stress by the plasma flow) F_{drg},
- inertial force F_{inr},
- Marangoni effects trough driven flows inside of the drop F_{mar}

and the remaining forces are

- surface tension effect F_γ and
- vapor jet force F_{vap}.

Former theoretical models are based on the static force balance model (SFBT) [18,31] or the pinch instability theory (PIT) [1,26]. Figure 9 shows a comparison between experimental and theoretical results for the drop diameter R_{drp} achieved in [18]. Agreement can be achieved with SFBT for currents lower 210 A, but it fails for high currents. PIT shows an opposite behavior, the theory is applicable for currents $\geq$ 250 A. Both theories are restricted to a small range of the welding parameters. The observed problem can be explained by the fact that the significant dynamic behavior of the GMAW process is neglected by SFBT and PIT. As a remedy, a dynamic drop-detachment model (DDM) based on the following assumptions will be proposed.

- computation domain is restricted to electrode wire and pendent drops
- position of the melting interface is given

- axisymmetric shape and motion of the drop
- isothermal domain
- neglect of internal rotational flows
- neglect of the direct dependence of the geometry on the spatially distributed forces
- constant values for surface tension, viscosity, and density
- constant welding current and wire feed speed

The basic idea of DDM consists in the simulation of a drop growth and detachment cycle in the steps

1. computation of the sum of the spatially distributed forces acting on the drop from first principles,
2. prediction of an a priori shape approximation determined by these forces using the static equilibrium theory, and
3. adjustment of the drop shape by simulating the dynamic response of the center of mass

where the melting rate of the electrode is considered by a drop volume growing from time step to time step. DDM uses a switch between the three cases where the drops are

- attached to the electrode with no neck (see truncated ellipsoid in Figure 10),
- attached with a neck (see truncated-ellipsoid/polynomial volume model of a necking drop in Figure 11), and
- detached from the electrode (full ellipsoid).

In each time step of the discrete simulation a decision has to be made which volume shape will be used to model the drop. Truncated ellipsoids are used initially and when the balance of forces at the liquid–solid boundary becomes less than zero, truncated ellipsoids and polynomial volumes are then used, which allows the formation of a neck. The final collapse of the drop neck represents the imbalance between the

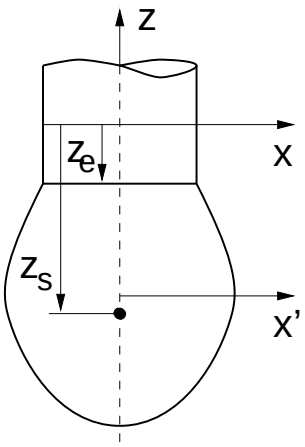

Figure 10: Truncated-ellipsoid model of drop with no neck (after [10])

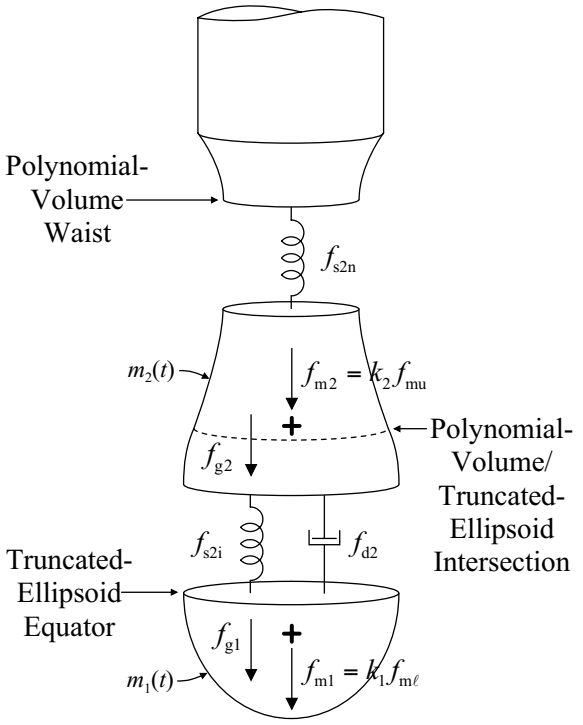

Figure 11: Truncated-ellipsoid/polynomial volume model of a necking drop (from [10])

primary forces acting on the drop just before detachment, namely magnetic forces and surface tension in the range of higher currents. The force balance F_{intf} at the melting interface is given as

$$F_{intf} = F_\gamma - F_{spr} - F_{dmp} + F_{mag} - K_{pr}\,. \quad (1)$$

The retaining surface tension force F_γ is computed with

$$F_\gamma = 2\pi R_{el}\gamma \sin\beta \quad (2)$$

where R_{el} is the wire radius, γ the interfacial surface tension between liquid metal and ionized gas, and β the tangent angle of the truncated ellipsoid at the electrode (cf. Figure 11).

F_{spr} and F_{dmp} are the spring and damping forces acting on the center of drop mass. The effect of surface tension on the motion of the center of drop mass is modeled as a non-linear spring with one end of the spring attached to the center of mass and the other end anchored to the solid electrode. Motions of the drop are damped by loss mechanisms in the fluid such as viscous losses and joule heating from eddy currents induced by fluid motion through the welding current's magnetic field. The magnetic force F_{mag} is that acting on the ellipsoid above its equator and was shown in [11] to be negative in argon-rich plasmas. A detailed description of the computation of F_{spr}, F_{dmp}, and F_{mag} is given in [10].

Finally, the term K_{pr} is an adjustable parameter to match the moment of neck formation with that observed in experiments. It is believed that this parameter models radial magnetic pressure acting on the drop.

3.2 Results

The model performance was successfully tested for different parameter sets covering

- drop dynamic for an attached drop,
- drop impulse response,
- drop dynamic for necking drops, and
- drop dynamic for free drops.

The DDM simulations were compared with measurements of obtained from video images over a range of welding currents.

For low currents where the drops are large and the magnetic forces are relatively small, the force balance in Eq. 1, which determines the transition from truncated ellipsoids to truncated ellipsoids/polynomial volumes, is not critical since the drop usually stays on the electrode for some time after the transition. The forces acting on the truncated ellipsoids and polynomial volumes are what then determines the time at which the drop detaches from the electrode. However, at higher currents in the globular transfer region where the drops are small and the magnetic forces are relatively large, the drop detaches soon after the transition from truncated ellipsoids to truncated ellipsoids/and polynomial volumes, and the time of the transition, determined by the force balance in Eq. 1, becomes more important.

Selected examples of simulations along with the equivalent experimental images are shown in Figure 12–16. A comparison of the impulse response of the model to measured responses of the drop is given in Figure 12. The welding arc was initially operated at a base current of 40 A with 330 A impulses superimposed at 5 Hz and a 2% duty cycle. A drop was ejected from the electrode with each current pulse. The peak current level was then briefly reduced to 260 A such that a drop was not ejected and a drop impulse response was observed. The comparison of the equatorial radius is shown in the upper graph. Of interest here are the oscillation frequency and damping rate. The surface tension, damping, and gravitational forces generated by the model are shown in the lower graph; the non-linear nature of the surface tension model is apparent. Magnetic forces are insignificant during the oscillation as the base current was only 40 A during this time. It was necessary to use a surface-tension coefficient approximately one-half the known value for molten steel and a relatively large damping coefficient. It is hypothesized that these discrepancies are due to fluid flow inside the drop and the model suggests that the effects of this flow are significant.

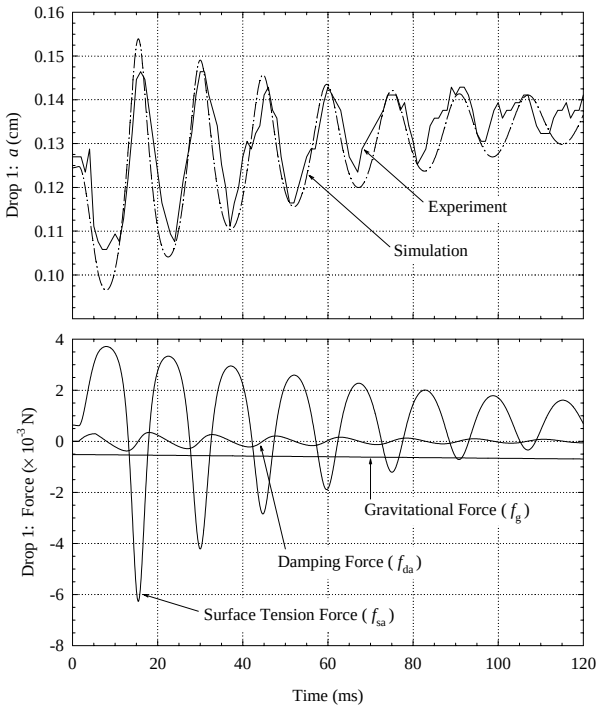

Figure 12: Drop impulse simulation (from [10])

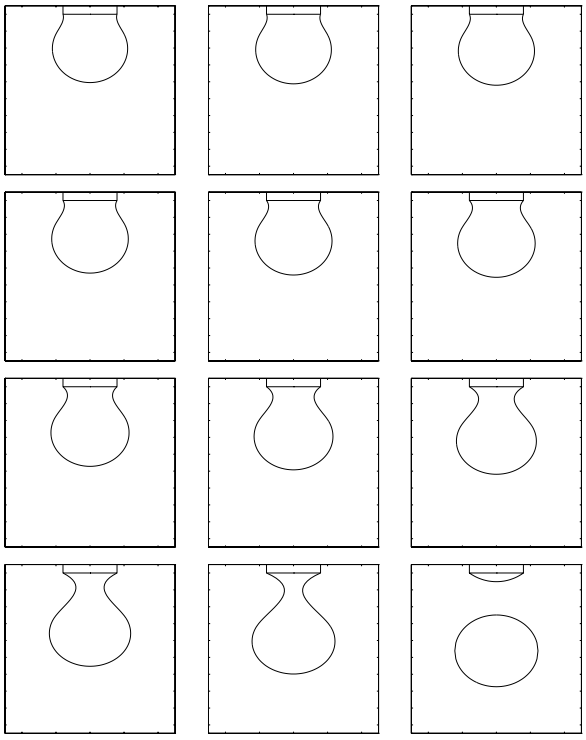

Figure 13: Simulated detachment, I=220 A, U=29 V, image interval = 4 ms (from [10])

The excess viscous losses may be the result of rotational flow in the drop driven by rotational components of magnetic body forces and Marangoni flow (flow driven by surface tension gradients). This rotational flow would result in additional viscous losses. It would also increase eddy current losses.

The simulated drop geometries for a constant current detachment compare well with the experimentally observed shapes. In Figure 13 and 14 the results for a current of 220 A are given. In particular, the model reproduces the oblate shape of the drop as it detaches from the electrode. The model is also able to predict drop shape and frequency with a high precision for higher currents. The results for computation and experiment in Figure 15 and 16 confirm this. The simulated drop detachment frequencies as a function of the current are shown in Figure 17.

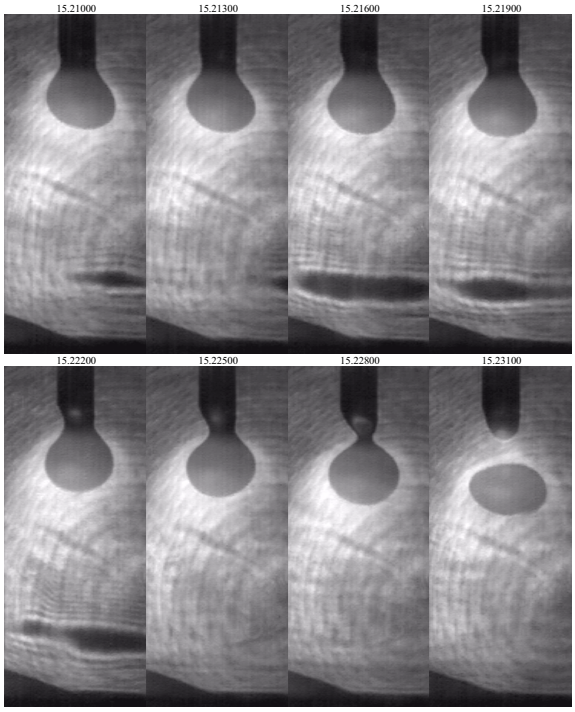

Figure 14: Measured detachment, I=220 A, U=29 V, image interval = 3 ms (from [10])

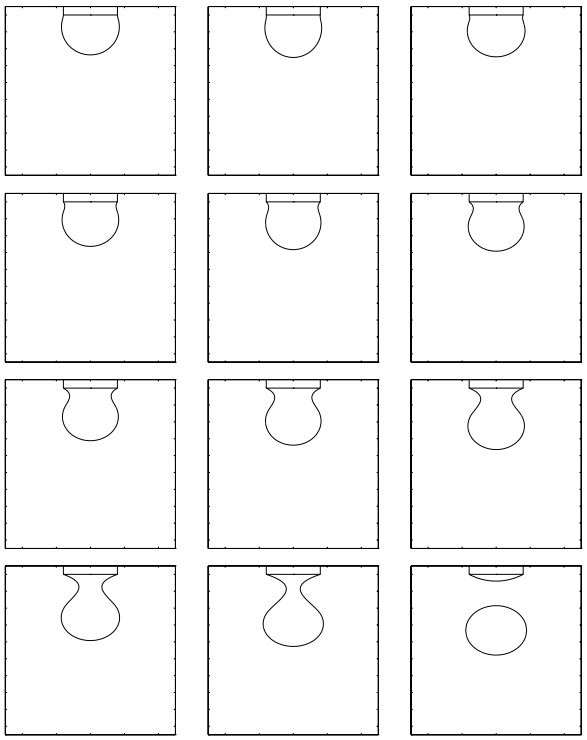

Figure 15: Simulated detachment, I=280 A, U=29 V, image interval = 4 ms (from [10])

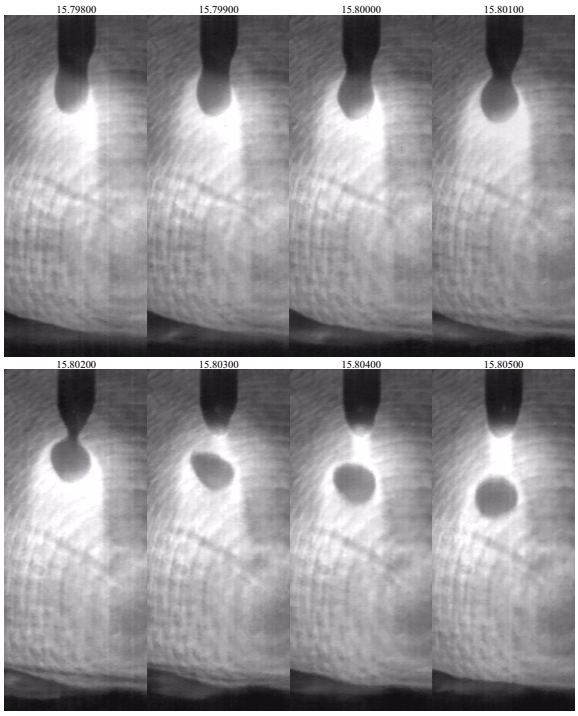

Figure 16: Measured detachment, I=280 A, U=29 V, image interval = 1 ms (from [10])

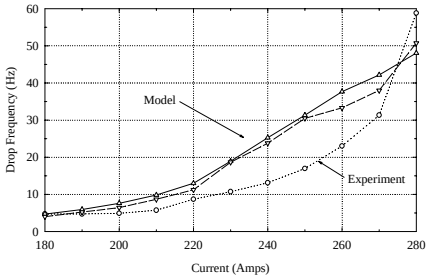

Figure 17: Simulated detachment frequencies (from [10])

3.3 Discussion

A dynamic model of drop detachment in GMAW was presented. It has the capability to demonstrate the significance of different physical effects including process dynamics (influence of gravity, magnetic forces, drop acceleration in the plasma, throwing off of drops by electrode vibration, etc) in a wide range of welding parameters. This capability allows e.g. to provide quantitative explanations for the effectiveness of current pulsing.

Simulations performed with this model are compared with measurements of welding images for low and moderate welding currents in an argon-rich plasma. An agreement between theoretical and experimental results for drop detachment could be achieved for a wide range of parameters. The comparisons indicate that the experimental magnetic forces are much less potent than the calculated magnetic forces when welding-current transients are not present. A hypothesis to explain this finding is that internal flows are able to develop under the relatively quiescent conditions that exist during drop development in constant-current welding.

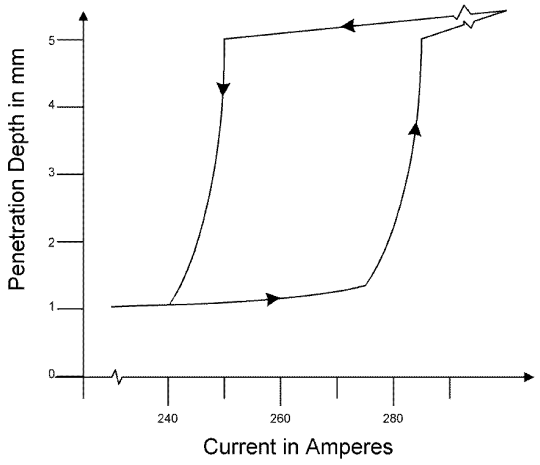

Figure 18: Variation of penetration depth with current for GTAW (after Lin and Eagar [22])

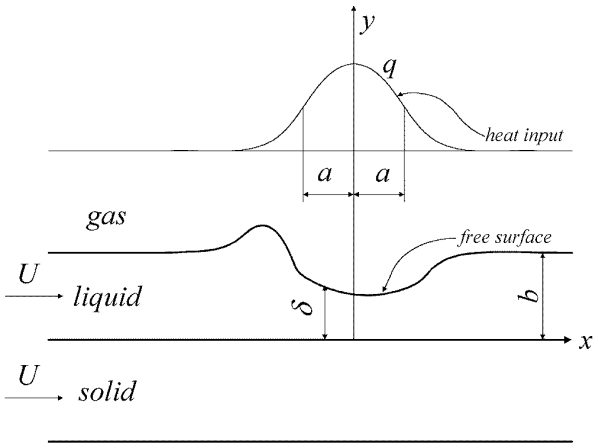

Figure 19: Problem studied: a moving liquid film under a heat source

4 Weld Pool Behavior

In this section we will investigate the role of Marangoni forces as the possible cause of deep penetration. The model presented is a simplified representation of the physics in the weld pool and depends critically on the mass and heat flow resulting from the perocess at the electrode.

In the high current regime (generally above 250 A), unexplained phenomena affect weld penetration, thus making the process uncertain and/or unreliable. Figure 18 shows previous work by Lin and Eagar [22], where a critical change in penetration with welding currents appears clearly. Current modeling efforts claim to be able to understand the lower penetration side of the curve (low currents), but the models break down as current increases beyond a critical point, and the surface deformation is large. Arc pressure itself cannot explain the magnitude of surface deformation, neither can evaporation forces, and our previous work [24] indicates that for GMAW, droplet impingement is not an important factor either.

4.1 Thermal and fluid flow model

In this study we focus on a two-dimensional liquid film that is moving under a linear gaussian heat source. Marangoni forces, fluid flow and heat transport are considered. Surface energy influence on free surface shape has been neglected, as well as electromagnetic effects and conduction heat transfer in the direction of the flow. In addition, the material is treated as a pure element, with a clearly defined melting point.

Experimental observation of welding at high currents showed the bottom of the weld pool presenting a "dry" aspect, that is, the bottom of the weld pool looked rough, instead of mirror-like typical of molten metal free surface. This evidence could indicate the presence of a film layer so thin that its free surface is affected by the roughness of the mushy zone. To understand the behavior of a thin layer, we will study a similar problem, that is not an accurate description of a welding process, but will give insight about the role of Marangoni forces in the deformation of a free surface. Figure 19 shows a schematic of the process analyzed. The problem described in Figure 19 is two-dimensional, and corresponds to the fluid flow, free surface deformation and energy transport in a thin film that is moving under a linear gaussian heat source.

Far from the heat source the film thickness is constant (b), and both the liquid and the solid and move towards the heat source at the same velocity U and temperature T_m.

4.2 Governing equations and boundary conditions

Asuming two-dimensional fluid and heat flow, constant properties, uniform pressure distribution, very low Reynolds number, and a surface heat source, the applicable forms of the momentum and energy equations are:
Momentum and Continuity:

$$\Psi_{\eta\eta\eta} = 0 \tag{3}$$

Boundary conditions:

$$\begin{cases} \Psi(\xi,0) &= 0 \\ \Psi_\eta(\xi,0) &= -\Delta(\xi) \\ \Psi(\xi,1) &= -1 \end{cases} \tag{4}$$

The order of the differential equation in η has been reduced from 4^{th} to 3^{rd} order. This has an important implication: we have now more boundary conditions that degrees of freedom. For this reason, Marangoni stresses will not be considered as a boundary condition now, and the corresponding Eq. 10 will be used as a check in an iterative method. The non-dimensional form of the Marangoni boundary condition is:

$$\Delta' f + \Delta f' + \tfrac{1}{2}\varphi' = \frac{2(1-\Delta)\sqrt{1+\Delta^2}}{S\Delta^2} \tag{5}$$

For the equation of conservation of energy, a large Peclet number will be assumed. The equation of energy in its dimensionless form then becomes:
Conservation of Energy:

$$\Phi_{\eta\eta} - \Delta Pe(\Phi_\eta \Psi_\xi - \Phi_\xi \Psi_\eta = 0) \tag{6}$$

Boundary conditions:

$$\begin{cases} \Phi(\xi,0) &= 0 \\ \Phi_\eta(-\infty,\eta) &= 0 \\ \Phi(\xi,1) &= \Delta(\xi)\, f(\xi) \end{cases} \tag{7}$$

where:

$$f(\xi) = C \exp\left(-\frac{\xi^2}{2\sigma^2}\right) \tag{8}$$

The independent variables are $\xi = x/b$ and $\eta = y/\delta(x)$ where b is the liquid layer thickness far from the heat source and δ is the surface deformation. The dimensionless dependent variables are Ψ and Φ defined as $\Psi = \psi/(Ub)$ and $\Phi = (T - T_m)/(T_m - T_\infty)$ where U the traveling velocity, T is the unknown temperature, T_m the melting temperature, and T_∞ the room temperature.

The Reynolds number, Peclet number and local liquid layer thickness ratio are defined by $Re = Ub/\nu$, $Pe = Ub/\alpha$ and $\Delta(\xi) = \delta(x)/b$, where ν the kinematic viscosity, and α heat diffusivity of the liquid layer. And additional dimensionless parameter, the surface tension number $S = C_\gamma(T_m - T_\infty)/(\mu U)$ is introduced where C_γ is the surface tension coefficient and μ the viscosity.

4.3 Solution procedure

The solution of the transformed equation of conservation of mass and momentum Eq. 3 is:

$$\Psi(\xi,\eta) = -\Delta\eta - (1-\Delta)\,\eta^2 \tag{9}$$

The transformed equation of energy will be solved approximating the temperature profile with a second order polynomial, and performing a shell balance at each point of the x coordinate. The following differential equation is obtained:
Conservation of energy:

$$A_1\phi' + A_2\phi + A_3 = 0 \tag{10}$$

Boundary condition:

$$\varphi(-\infty) = 0 \tag{11}$$

where:

$$\begin{cases} A_1 &= -\Delta Pe\,(5-\Delta)\,/\,12 \\ A_2 &= -(1 - \Delta\Delta' Pe\,/\,12) \\ A_3 &= \Delta Pe\,(\Delta\Delta' f - 2\Delta f' + \tfrac{1}{2}\Delta^2 f \\ & \quad -2\Delta' f)\,/\,3 \end{cases} \tag{12}$$

The Marangoni condition can be expressed as:

$$\varphi = \frac{A1}{A2}\left[2\Delta' f + 2\Delta f' - \frac{4\,(1-\Delta)\sqrt{1+\Delta^2}}{S\Delta^2}\right] - \frac{A_3}{A_2} \quad (13)$$

The solution of the coupled problem consists on finding the two functions $f(x)$ and $D(x)$ that satisfy the energy equation Eq. 10 and the Marangoni condition Eq. 13 simultaneously. In this work domain of x was discretized in 100 intervals (101 nodes). The iterative algorithm used to find the two functions is the following:

1. assigning a value to Δ for each of the nodes
2. integrating the equation of energy for φ_E
3. calculating φ_M from the Marangoni condition
4. comparing φ_E and φ_M
5. assigning a new value to Δ for each of the nodes

4.4 Order of magnitude estimation

A simplified analysis for the deepest part of the weld pool yields an approximate estimation of the minimum molten metal film thickness:

$$\delta^* = \left(-4\frac{abU}{q_{max}}\frac{\mu k_l}{C_\gamma}\right)^{1/3} \quad (14)$$

where a is the standard deviation of the heat source, q_{max} the maximum heat input, and k_l the heat conductivity of the liquid.

4.5 Results

The material considered for this example is pure aluminum. The thermophysical properties used are summarized in Table 2. The process parameters are summarized in Table 3. Using this values the Peclet number is 0.71 and the Reynolds number 36.

Figure 20 summarizes the results of the model. The free surface has a hump at the front end and is greatly depressed under the

Table 2: Material Properties for Pure Aluminum

Symbol	Value	Units
C_γ	$-3.6 \cdot 10^{-4}$	N/(m K)
c_p	682	J/(kg K)
k_l	70	W/(m K)
T_m	650	^{o}C
ϱ	2700	kg/m^3
μ	$2 \cdot 10^{-3}$	Pa s

Table 3: Process Parameters

Symbol	Value	Units
a	10^{-3}	m
b	$1.5 \cdot 10^{-3}$	m
q_{max}	$6.65 \cdot 10^6$	W/m^2
T_∞	25	^{o}C
U	$1.8 \cdot 10^{-2}$	m/s

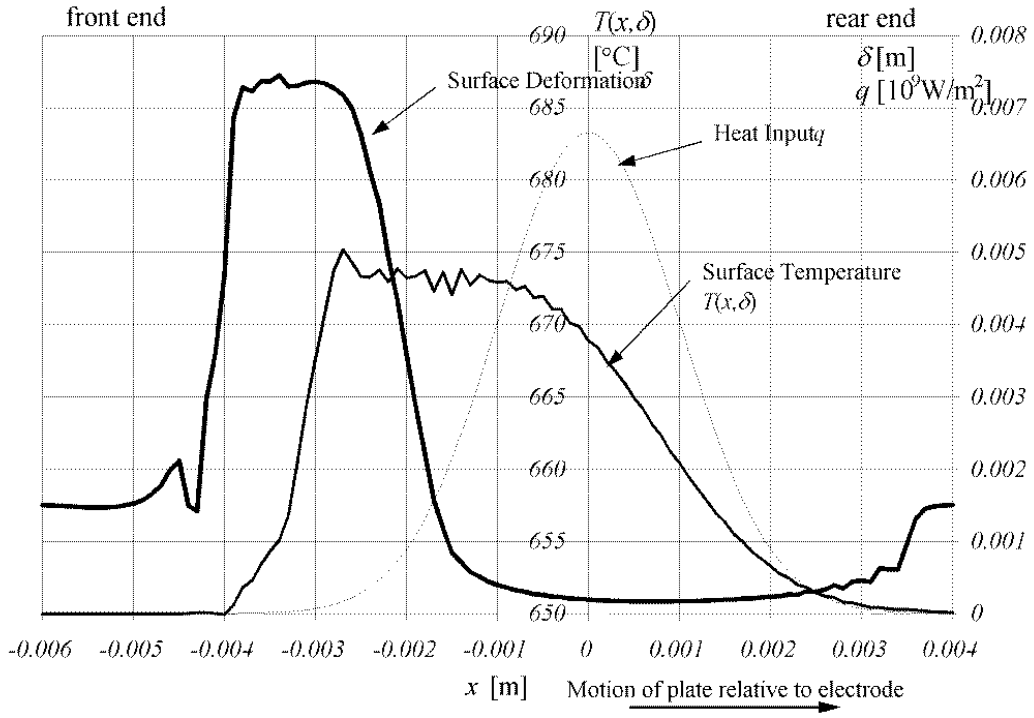

Figure 20: Surface deformation, temperature and heat input for the case of study

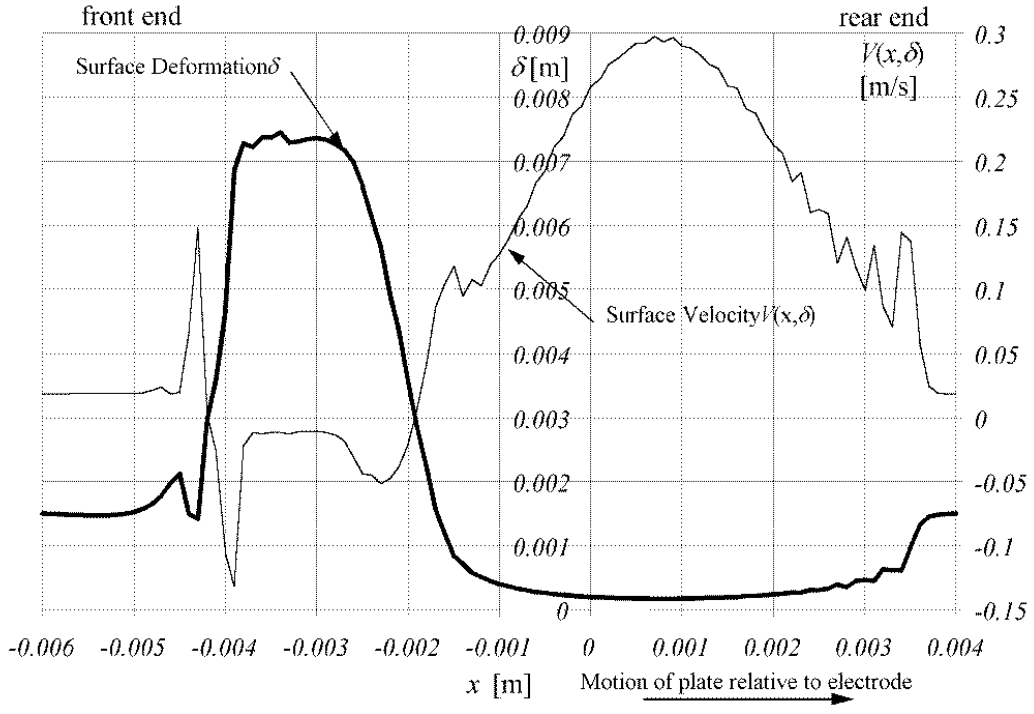

Figure 21: Surface deformation and velocity for the case of study

Table 4: Comparison of semi-analytical and order of magnitude results

	Equ.	Semi-analytical	Order of Magnitude	Unit
$delta^*$	9	$1.71 \cdot 10^{-4}$	$1.85 \cdot 10^{-4}$	m
T^*	5	25.2	17.6	^{o}C
V^*	7	0.297	0.309	m/s

heat source. The surface temperature rises in front the heat source. Some numerical oscillations can be observed at the beginning of the hump of the surface and at the highest surface temperatures. Figure 21 shows the calculated surface velocity. At the deepest part of the depression it reaches values of the order of 0.3 m/s. It is evident also that the hump at the front end of the weld corresponds with negative surface velocities. Some numerical oscillations are observed at the beginning of the front hump and at the rear end of the weld. The surface velocity is the resultant of its components in x and y directions. Table 4 summarizes the results obtained using the order of magnitude calculations and the semi-analytical model.

4.6 Discussion

The results obtained indicate that indeed, Marangoni stress can cause surface depression and induce high velocities in the melt. For the point of most interest, the point of maximum surface depression, the order of magnitude calculations actually give results very similar to the semi-analytical model. A film thickness of the order of tenths of a millimeter would be consistent with the observation of a rough surface at the bottom of the weld pool, since such a thin film would follow the roughness of the mushy zone in an alloy. The velocities obtained are similar to those usually reported in the literature. The 7 mm high hump at the front end of the weld pool does not correspond with usual welding experiences. The most likely reason the size of that hump was overestimated is that the flattening effect of surface tension and hydrostatic pressure were neglected. Other possibility could be that the magnetic forces exert a restorative action on the surface.

4.7 Conclusions and Recommendations

This work supports the possibility that large depressions of the weld pool during welding are due to the strong effect of Marangoni shear stress. In these cases the weld pool would acquire the configuration of a thin film under the arc. This could explain why other numerical models break down at higher currents, and why there is a sharp transition in penetration with current as reported by Eagar and Lin. Extension of this mechanism to a three-dimensional problem could shed some light in the phenomenon of undercutting. Coupled with the proper thermal model for the solid state this approach can be used to study welding in thin sheet. The equations used can be extended to include melting and solidification by only changing the boundary conditions. Also the geometry can be adapted to a non flat interface, as long as the liquid can still be considered a thin film. The hypotheses stated initially are valid for the deepest part of the surface, therefore an experimental validation of the results would be the most valuable next step. In next revisions of the calculations, consideration of surface tension effects, and finite Peclet and Reynolds numbers would be for further study

5 Concluding Remarks

The effect of drop dynamics and Marangoni driven weld pool flows in GMAW has been investigated. Some important conclusions can be drawn:

- Although GMAW is a complex process, order of magnitude estimates and simple models can help to determine the relevant physics.

- Fluid flow in both the drop and in the weld pool has a major influence on weld quality.
- Understanding the physics permits improvement in weld quality, design of better power supply, and reduction of fume formation.

Acknowledgements

Support for this work was provided by the United State Department of Energy, Office of Basic Engineering Sciences. The work of one of the authors (D.W.) was support by the Deutscher Akademischer Austauschdienst (DAAD) in the framework of the NATO Science Fellowships Program.

References

[1] C. J. Allum. Metal transfer in arc welding as a varicose instability: I. Varicose instabilities in a current-carrying liquid cylinder with surface charge. *J. Phys. D: Appl. Physics*, 18:1431–1446, 1985.

[2] H. K. D. H. Bhadeshia. Possible effects of stress on steel weld microstructures. In *Proc. of the 2nd Int. Seminar on Mathematical Modelling of Weld Phenomena*, pages 207–225, Graz-Seggau, Austria, May 1993.

[3] Y. Chen, T. Zacharia, and S. A. David. Heat transfer and fluid flow in gas metal arc (GMA) weld pool with free surface. In *Proc. of the AWS Convention, Los Angeles, CA*, April 1997.

[4] S. K. Choi, C. D. Yoo, and Y.-S. Kim. Effect of pulse current on metal transfer of an arc electrode trough dynamic simualtion. In *Proc. of the AWS Convention, Los Angeles, CA*, April 1997.

[5] R. T. Choo and J. Szekely. The effect of gas shear stress on marangoni flows in arc welding. *Welding Journal*, pages 223s–233s, September 1991.

[6] R. T. Choo and J. Szekely. Vaporization kinetics and surface temperature in a mutually coupled spot gas tungsten arc weld and weld pool. *Welding Journal*, pages 77s–93s, March 1992.

[7] J. Goldak et al. Modeling the slit test for assessing sensitivity to hydrogen cracking. In T. Zacharia, editor, *Proc. of the Int. Conf. on Modeling and Control of Welding Processes*, pages 161–173. AWS, 1994.

[8] J. Goldak and M. Gu. Computational weld mechanics of the steady state. In *Proc. of the 2nd Int. Seminar on Mathematical Modelling of Weld Phenomena 2*, pages 207–225, Graz-Seggau, Austria, May 1993.

[9] P. R. Heald, R. B. Madigan, T. A. Siewert, and S. Liu. Droplet transfer modes for a MIL 100S-1 GMAW electrode. Technical Report NISTIR 3976, U.S. Department of Commerce, October 1991.

[10] L. A. Jones, T. W. Eagar, and J. H. Lang. A dynamic model of drops detaching from a gas metal arc welding electrode. *submitted to J. Phys. D: Appl. Phys.*, 1997.

[11] L. A. Jones, T. W. Eagar, and J. H. Lang. Magnetic forces acting on molten drops in gas metal arc welding. *submitted to J. Phys. D: Appl. Phys.*, 1997.

[12] L. A. Jones, T. W. Eagar, and J. H. Lang. The temporal nature of forces acting on metal drops in gas metal arc welding. In *Proc. of the 14th Symposium on Energy Engineering Sciences, Argonne, IL*, May 1997.

[13] P. G. Jönsson, J. Szekely, R. T. C. Choo, and T. P. Quinn. Mathematical models of transport phenomena associated with arc-welding processes: a survey. *Modelling Simul. Mater. Sci. Eng.*, 2:995–1016, 1994.

[14] P. G. Jönsson, R. C. Westhoff, and J. Szekely. Arc characteristics in gas-metal arc welding of aluminum using argon as the shielding gas. *J. Appl. Phys.*, 74(10):5997–6006, November, 1993.

[15] J. W. Kim and S. J. Na. A study on the effect of contact tube-to-workpiece distance on weld pool shape in gas metal arc welding. *Welding Journal*, pages 141s–152s, May 1995.

[16] Y. S. Kim. *Metal Transfer in Gas Metal Arc Welding*. PhD thesis, MIT, DMSE, Cambridge, MA, 1989.

[17] Y.-S. Kim and E. T. Eagar. Analysis of metal transfer in gas metal arc welding. *Welding Journal*, 72(269s–178s), 1993.

[18] Y.-S. Kim and T. W. Eagar. Metal transfer in pulsed current gas metal arc welding. *Welding Journal*, pages 279s–287s, July 1993.

[19] W. Kurz and R. Trivedi. Modern solidification theory applied to welding. In *Proc. of 4th Int. Conf. on Trends in Welding Research, Gatlinburg, TN*, pages 115–120, 1995.

[20] J. F. Lancaster. *The Physics of Welding*. Pergamon Press, Oxford, GB, 2nd edition, 1986.

[21] K. N. Lankalapalli, J. F. Tu, and M. Gartner. A model for estimating penetration depth of laser welding processes. *J. Phys. D: Appl. Phys. 29*, pages 1831–1841, 1996.

[22] M. L. Lin and T. W. Eagar. Influence of arc pressure on weld pool geometry. *Welding Journal*, pages 163s–169s, June 1985.

[23] J. J. Lowke, R. Morrow, and J Haidar. A simplified unified theory of arcs and their electrodes. *J. Phys. D: Appl. Phys.*, 30:1–30, 1997.

[24] P. Mendez. Unbublished report. MIT, DMSE, Cambridge, MA, 1997.

[25] V. Michailov, J. Ruge, and K. Thomas. Berechnung der Wasserstoffverteilung beim Schweißen. *Schweißen und Schneiden*, 43(11):655–658, 1991. (in German).

[26] V. A. Nemchinsky. Size and shape of the liquid droplet at the molten tip of an arc electrode. *J. Phys. D: Appl. Phys.*, 27:1433–1442, 1994.

[27] V. A. Nemchinsky. The effect of the type of plasma gas on current constriction at the molten tip of an arc electrode. *J. Phys. D: Appl. Phys.*, 29:1202–1208, 1996.

[28] D. Radaj. Potential of numerical analysis of weldability in the design process. In *Proc. of the 2nd Int. Seminar on Numerical Analysis of Weldability*, pages 1–17, Graz-Seggau, Austria, May 1993.

[29] V. A. Sudnik. Modelling of MAG process. In *Proc. of the 3rd Int. Seminar on Numerical Analysis of Weldability, Graz-Seggau, Austria*, September 1995.

[30] W. Sudnik, D. Radaj, and W. Erofeew. Computerized simulation of laser beam welding, modelling and verfication. *J. Phys. D: Appl. Phys.*, 29:2811–2817, 1996.

[31] A. D. Watkins, H. B. Smartt, and J. A. Johnson. A dynamic model of droplet growth and detachment in GMAW. In A. A. David and J. M. Vitek, editors, *Proc. of the Conf. on Int. Trends in Welding Science and Technology*, pages 993–997, 1993.

[32] D. Weiss, U. Franz, and J. Schmidt. Simulation of the weld pool formation during vertical arc welding with emphasis on the influence of groove preparation. In *Proc. of the* 6^{th} *Int. Conf. on Computer Technology in Welding, Lanaken, Belgium*, June 1996.

[33] R. Westhoff. *Modeling of the Non-transfered Arc Plasma Torch and Plume for Plasma Processing*. PhD thesis, MIT, Cambridge, MA, 1992.

[34] T. Zacharia, A. H. Eraslan, and D. K. Aidun. Modeling of non-autogenous welding, model predicts three-dimensional convection and temperature conditions of the weld pool generated by a moving arc. *Welding Journal*, pages 18s–27s, January 1988.

[35] P. Zhu, J. J. Lowke, R. Morrow, and J. Haidar. Prediction of anode temperatures of free burning arcs. *Journal of Physics D: Applied Physics*, 28(1369–1376), 1995.